iRHOM2 regulates inflammation and endothelial barrier permeability via CX3CL1

HUIYUAN YAN[1], JUNSONG WU[2] and HUILIAN YAN[3]

[1]Department of Internal Medicine, Children's Hospital of Fudan University, Shanghai 201102; [2]Medical College, Qinghai University, Xining, Qinghai 810016; [3]Fenyang College, Shanxi Medical University, Taiyuan, Shanxi 030604, P.R. China

Received September 14, 2022; Accepted February 16, 2023

DOI: 10.3892/etm.2023.12018

Abstract. Acute lung injury (ALI) is associated with increased lung inflammation and lung permeability. The present study aimed to determine the role of inactive rhomboid-like protein 2 (iRHOM2) in ALI in lipopolysaccharide (LPS)-induced pulmonary microvascular endothelial cell model. Human pulmonary microvascular endothelial cells (HPMVECs) were transfected with small interfering RNA targeting iRHOM2 and C-X3-C motif chemokine ligand 1 (CX3CL1) overexpression plasmids and treated with LPS. Cell viability was detected using a Cell Counting Kit-8 assay, while levels of TNFα, IL-1β, IL-6 and p65 were measured by reverse transcription-quantitative PCR and western blotting. Apoptosis levels were measured using a TUNEL assay. Endothelial barrier permeability was detected, followed by analysis of zonula occludens-1, vascular endothelial-cadherin and occludin by immunofluorescence staining or western blotting. The interaction of iRHOM2 and CX3CL1 was analyzed using an immune-coprecipitation assay. Through bioinformatics analysis, it was found that CX3CL1 was upregulated in the LPS group compared with the control. Kyoto Encyclopedia of Genes and Genomes pathway analysis demonstrated that the TNF signaling pathway affected by iRHOM2 and cytokine-cytokine receptor interaction, including CX3CL1, served a key role in ALI. HPMVECs treated with LPS exhibited a decrease in cell viability and an increase in inflammation, apoptosis and endothelial barrier permeability, while these effects were reversed by iRHOM2 silencing. However, CX3CL1 overexpression inhibited the effects of iRHOM2 silencing on LPS-treated HPMVECs. The present study demonstrated a novel role of iRHOM2 as a regulator that affects inflammation, apoptosis and endothelial barrier permeability; this was associated with CX3CL1.

Correspondence to: Dr Huiyuan Yan, Department of Internal Medicine, Children's Hospital of Fudan University, 399 Wanyuan Road, Minhang, Shanghai 201102, P.R. China
E-mail: yanhuiyuan2@126.com

Key words: acute lung injury, inactive rhomboid-like protein 2, C-X3-C motif chemokine ligand 1, inflammation, oxidative stress

Introduction

Acute lung injury (ALI) is an acute progressive hypoxic respiratory failure caused by external and external pathogenic factors other than cardiogenesis. ALI is a syndrome of increased lung inflammation and permeability (1). On one hand, LPS stimulation increases the permeability of human pulmonary microvascular endothelial cells (HPMVECs) and causes protein exudation and edema. On the other hand, lipopolysaccharide (LPS) stimulates endothelial cells to secrete inflammatory cytokines and other adhesion molecules, which induces aggregation of a large number of neutrophils and leads to oxidative damage and the inflammatory response in lung tissue, promoting the development of lung injury (2-4). TNF-α, IL-1β and IL-6 are the primary pro-inflammatory factors in the early development of ALI, which not only directly cause lung injury, but also activate other signaling pathways and promote expression of inflammatory factors, leading to lung injury (5).

Inactive rhomboid-like protein 2 (iRHOM2) is a member of the rhomboid protein family, of which >10 members have been identified (6). iRHOM2 promotes atherosclerosis by inducing macrophage inflammation and oxidative stress; interfering with iRHOM2 decreases obesity by increasing thermogenesis (7,8). In addition, iRHOM2 is involved in promoting particulate matter 2.5-induced chronic kidney injury and promotes lupus nephritis via TNFα and EGFR signaling (9). iRHOM2 silencing decreases LPS-induced inflammatory release of cardiomyocytes (10). A previous study demonstrated that iRHOM2 alleviates lung injury caused by intestinal ischemia-reperfusion (11). Therefore, the present study aimed to explore if iRHOM2 is involved in lung microvascular endothelial cell injury.

Materials and methods

Bioinformatics analysis

Data source. The National Center for Biotechnology Information-Gene Expression Omnibus database (ncbi.nlm.nih.gov/geo/) is a free database of microarray/gene profile and next-generation sequencing data from which gene expression profile data (accession no. GSE5883) of human lung microvascular endothelial cells exposed to LPS were obtained in the present study.

Identification of differentially expressed genes (DEGs). DEGs were identified between the LPS 4 hrs and CTL 4 hrs groups in the aforementioned dataset using the 'limma' R package as previously described (12). Statistically significant DEGs were determined with adjusted P-value (adj.P-value)<0.01 as the cut-off criterion. The analysis results were presented using a volcano plot and heatmap.

Biological function analysis. Using Gene Ontology (GO) enrichment analysis (http://geneontology.org/docs/go-enrichment-analysis/), the biological function, pathway or cell location of enriched genes was identified. The GO annotation contains three aspects of biological content: i) Biological process (BP); ii) cellular component (CC) and iii) molecular function (MF). By analyzing the genes in the Kyoto Encyclopedia of Genes and Genomes (KEGG, https://www.kegg.jp/) signaling pathways, the pathways that were altered under disease conditions were identified. The present study used R package 'Org.Hs.eg.db' (13) to perform GO functional annotation and KEGG pathway analysis of differential expressed immune-related genes (DEIRGs).

Construction of the protein-protein interaction (PPI) network. Search Tool for the Retrieval of Interacting Genes/Proteins (STRING) (14) online database was used to develop the PPI network. iRHOM2 and C-X3-C motif chemokine ligand 1 (CX3CL1) were uploaded to the STRING database and isolated nodes were removed from the network.

Cell culture. Immortalized HPMVECs were purchased from Sigma-Aldrich (cat. no. 540-05A; Merck KGaA) and cultured in RPMI-1640 medium (Thermo Fisher Scientific, Inc.) supplemented with 1% penicillin-streptomycin and 10% fetal bovine serum (HyClone; Cytiva) at 37˚C with 5% CO_2. The cells were treated with LPS (10 μg/ml) for 12, 24 or 48 h at 37˚C.

Cell transfection. For knockdown of iRHOM2, the specific small interfering (si)RNA targeting iRHOM2 (siRNA-iRHOM2#1, 5'-GCGUGAGAUGGUUGGUUAAGG-3'; siRNA-iRHOM2#2, 5'-GACGAUGUCUCAUGGAUUAAA-3') and corresponding negative control (NC) siRNA (5'-UUCUCCGAACGUGUCACGU-3') were synthesized by Shanghai GenePharma Co., Ltd. To overexpress CX3CL1, pc-DNA3.1 vector containing the whole length of CX3CL1 (Ov-CX3CL1) and empty vector (Ov-NC) were synthesized by Shanghai GeneChem Co., Ltd. A total of 100 nM recombinants were transfected into HPMVECs for 48 h at 37˚C using Lipofectamine® 2000 reagent (Invitrogen; Thermo Fisher Scientific, Inc.) according to the manufacturer's instructions. After 48 h, cells were collected for further assay.

Reverse transcription-quantitative PCR (RT-qPCR). RT-qPCR was used to detect mRNA expression levels. Total RNAs were extracted from $1x10^4$ HPMVECs using TRIzol® (Invitrogen; Thermo Fisher Scientific, Inc.), according to the manufacturer's instructions. All primers were designed and synthesized by Shanghai Sangong Pharmaceutical Co., Ltd. RT of first-strand cDNAs was performed by using PrimeScript™ RT Master Mix (Perfect Real Time; Takara Bio, Inc.), according to the manufacturer's instructions. Amplification of cDNA was performed using qPCR using the SYBR Premix Ex Taq™ II kit (Takara Bio, Inc.). The following thermocycling conditions were used for qPCR: Initial denaturation at 95˚C for 2 min, followed by 40 cycles of denaturation at 95˚C for 15 sec, amplification at 53˚C for 20 sec and extension at 60˚C for 3 sec. The following primer pairs were used: iRHOM2: Forward, 5'-TGGCCTGGAGCTGTCTATCT-3' and reverse, 5'-GTGATGGAGAGGTTGGGTGG-3'; TNFα: Forward, 5'-CTGGGCAGGTCTACTTTGGG-3' and reverse, 5'-CTGGAGGCCCCAGTTTGAAT-3'; IL-1β: Forward, 5'-AACCTCTTCGAGGCACAAGG-3' and reverse, 5'-AGATTCGTAGCTGGATGCCG-3'; IL-6: Forward, 5'-TCCACAAGCGCCTTCGGTC-3' and reverse, 5'-GGTCAGGGGTGGTTATTGCAT-3'; CX3CL1: Forward, 5'-TCCGATATCTCTGTCGTGGC-3' and reverse, 5'-TGTCTCGTCTCCAAGCAGC-3' and GAPDH: Forward, 5'-GGGAAACTGTGGCGTGAT-3' and reverse, 5'-GAGTGGGTGTCGCTGTTGA-3'. GAPDH was used as an internal reference and relative expression levels of target mRNAs were quantified using the $2^{-\Delta\Delta Cq}$ method (15).

Western blotting. Total protein of HPMVECs was extracted using RIPA buffer (Hunan Auragene Biotech Co., Ltd) and quantified using the BCA Protein Assay Kit (Beijing Dingguo Changsheng Biotechnology Co., Ltd.). The protein (20 μg per lane) in cell lysates was separated by 8% SDS-PAGE (Bio-Rad Laboratories, Inc.) and transferred onto PVDF membranes (MilliporeSigma; Merck KGaA). Subsequently, membranes were blocked in 5% non-fat milk for 1.5 h at room temperature and incubated with primary antibodies against iRHOM2 (1:1,000; cat. no. MAB10048; R&D Systems China Co., Ltd.), TNFα (1:1,000; cat. no. ab183218; Abcam), IL-1β (1:1,000; cat. no. ab216995; Abcam), IL-6 (1:1,000; cat. no. ab233706; Abcam), phosphorylated p65 (p-p65; 1:1,000; cat. no. ab76302; Abcam), p65 (1:1,000; cat. no. ab32536; Abcam), Bax (1:1,000; cat. no. ab32503; Abcam), Bcl-2 (1:1,000; cat. no. ab32124; Abcam), Cleaved caspase 3 (1:500; cat. no. ab32042; Abcam), zonula occludens-1 (ZO-1; 1:1,000; cat. no. ab221547; Abcam), vascular-endothelial (VE)-cadherin (1:1,000; cat. no. ab205336; Abcam), occludin (1:1,000, cat. no. ab242202; Abcam), CX3CL1 (1:1,000, cat. no. ab25088; Abcam) or GAPDH (1:1,000, cat. no. ab8245; Abcam) overnight at 4˚C. Following primary antibody incubation, membranes were incubated with HRP-conjugated anti-mouse (1:2,000; cat. no. ab6789; Abcam) or anti-rabbit (1:2,000; cat. no. ab6721; Abcam) secondary antibodies at 37˚C for 2 h. Then, protein bands were visualized using ECL Detection Reagent (Shanghai Yeasen Biotechnology Co., Ltd.) and densitometry analysis was performed using ImageJ software (version 1.49; National Institutes of Health).

Cell Counting Kit-8 (CCK-8) assay. HPMVECs were added to 96-well plates at a density of $5x10^3$ cells/well. The cells were placed in an incubator at 37˚C with 5% CO_2 for 24 h. Subsequently, 20 μl CCK-8 reagent (Beyotime Institute of Biotechnology) was added to each well. After 4 h, the absorbance at 450 nm was measured using a microplate reader.

TUNEL assay. TUNEL assay was used to detect apoptotic cells using a TUNEL kit (cat. no. C1082; Beyotime Institute of Biotechnology), according to the manufacturer's protocol. HPMVECs were fixed with 4% paraformaldehyde at room temperature for 15 min and permeated with 0.1% Triton

X-100 for 5 min at room temperature. Subsequently, cells were incubated with TUNEL at 37˚C for 1 h and cell nuclei were counterstained with DAPI (10 mg/ml; Koritai Biotechnology) for 5 min at room temperature. A total of five fields of view were randomly selected from each slice. The number of positive cells was mounted with fluorescent mounting media (Beijing Solarbio Science & Technology Co., Ltd.) and the observation was conducted under a fluorescence microscope (Nikon Corporation). The cell apoptosis rate (%) was calculated as follows: Number of apoptotic positive cells/total number of cells.

Measurement of endothelial barrier permeability. Transendothelial electrical resistance (TEER) is a key indicator for the detection of the integrative function of the monolayer cell barrier. It reflects the change in monolayer cell permeability by detecting the voltage difference between the inside and outside of the cell (16). TEER of HPMVECs was detected using a Millicdl ESR-2 cell resistance instrument (Millipore). TEER was determined using the following formula: TEER=($TEER_A$-$TEER_{blank}$) x $S_{membrane}$, where A is the TEER value for each Transwell filter and $S_{membrane}$ is the area of the filter membrane (S=π x r; r=6 mm).

Immunofluorescence (IF) assay. HPMVECs were fixed with 4% paraformaldehyde at 4˚C for 15 min and permeabilized with Triton X-100 at 37˚C for 30 min. Subsequently, cells were incubated with primary antibodies against ZO-1 (1:100; cat. no. ab221547; Abcam) at 4˚C overnight, and then incubated with Alexa Fluor 488-conjugated goat anti-rabbit IgG H&L secondary antibodies (1:500; cat. no. ab150077; Abcam) for 1 h at room temperature. Nuclei were stained with 1 μg/ml DAPI solution at room temperature for 15 min. The images were observed under a fluorescence microscope (magnification, x100).

Immunoprecipitation (IP) assay. The association between iRHOM2 and CX3CL1 was detected using IP assay. HPMVECs were collected and lysed using RIPA lysis buffer (Thermo Fisher Scientific, Inc.). Antibodies against iRHOM2 (1:500; cat. no. orb386934, Biorbyt, Ltd.), CX3CL1 (1:500; cat. no. 14-7986-81; Invitrogen; Thermo Fisher Scientific, Inc.) and IgG (1:200; cat. no. ab205718; Abcam) were added to the lysate for incubation at 4˚C overnight. Then, 40 μl Protein A/G PLUS-Agarose beads (Invitrogen; Thermo Fisher Scientific, Inc.) were added and incubated at room temperature for another 2 h. Then, the beads were rinsed with lysis buffer for three times and the collected by centrifugation at 12,000 x g for 2 min at 4˚C. Following the final wash, the supernatant was aspirated and discarded, then the precipitated proteins were re-suspended in 2 x SDS-PAGE loading buffer, boiled for 5min, and rinsed from the beads. The products from immunoprecipitation were collected for the analysis of iRHOM2 and CX3CL1 expression.

Statistical analysis. GraphPad Prism 8.0 statistical software (GraphPad Software, Inc.; Dotmatics) was used for statistical analysis. Data are presented as the mean ± standard deviation of three independent experiments. Differences between multiple groups were analyzed using one-way ANOVA followed by Tukey's post hoc test. R software version 3.6.3 was used for bioinformatics analysis (17). $P<0.05$ was considered to indicate a statistically significant difference.

Results

Identification of DEGs. Using adj. P-value <0.01 as the cut-off criterion, 203 DEGs were extracted from the expression profile dataset GSE5883, including 187 up- and 16 downregulated genes in the LPS 4 hrs group compared with the CTL 4 hrs group (Fig. 1A). A heatmap of the top 30 upregulated DEGs, which included CX3CL1, is shown in Fig. 1B. In the BP group, DEGs were mainly enriched in 'response to lipopolysaccharide', 'response to molecule of bacterial origin' and 'response to tumor necrosis factor' (Fig. 1C-F). In the CC group, DEGs were primarily enriched in 'membrane raft', 'membrane microdomain' and 'membrane region'. In the MF group, DEGs were primarily enriched in 'cytokine activity', 'cytokine receptor binding' and 'receptor ligand activity'. KEGG pathway analysis revealed that the DEGs were primarily enriched in 'TNF signaling pathway', 'cytokine-cytokine receptor interaction', 'Rheumatoid arthritis', 'IL-17 signaling pathway' and 'NF-kappa B signaling pathway'.

Identification of the interaction between iRHOM2 and CX3CL1 using a PPI network. To investigate the interaction between the gene iRHOM2 and CX3CL1, the STRING online tool was used to construct a PPI network (Fig. 1G). There was no direct association between iRHOM2 and CX3CL1.

iRHOM2 silencing increases HPMVEC viability induced by LPS. To analyze the role of iRHOM2 in ALI, HPMVECs were treated with LPS for 12, 24 or 48 h. LPS treatment induced a time-dependent increase in iRHOM2 expression at both mRNA and protein levels compared with that in the control group (Fig. 2A and B). HPMVEC viability was decreased by LPS treatment in a time-dependent manner (Fig. 2C). iRHOM2 silencing was induced in HPMVECs using siRNA targeting iRHOM2. The mRNA and protein expressions of iRHOM2 were decreased following iRHOM2 silencing compared with that in the siRNA-NC group (Fig. 2D and E). HPMVEC viability following LPS treatment was increased in the iRHOM2 silencing group compared with that in the siRNA-NC group (Fig. 2F).

iRHOM2 silencing decreases inflammation, apoptosis and endothelial barrier permeability in LPS-treated HPMVECs. The present study examined if iRHOM2 serves a role in inflammation and apoptosis associated with ALI. TNF-α, IL-1β and IL-6 levels were measured by RT-qPCR and western blotting. iRHOM2 silencing decreased the levels of TNF-α, IL-1β and IL-6 compared with those in the siRNA-NC group (Fig. 3A-B). As Fig. 3C depicted, the increased expression of p-p65 in LPS group was decreased by iRHOM2 silence. In addition, apoptosis levels were decreased in the iRHOM2 silencing group compared with those in the siRNA-NC group (Fig. 4A). Furthermore, the iRHOM2 silencing group showed increased Bcl-2 expression but decreased Bax and cleaved caspase3 expression compared with the siRNA-NC group (Fig. 4B). To determine

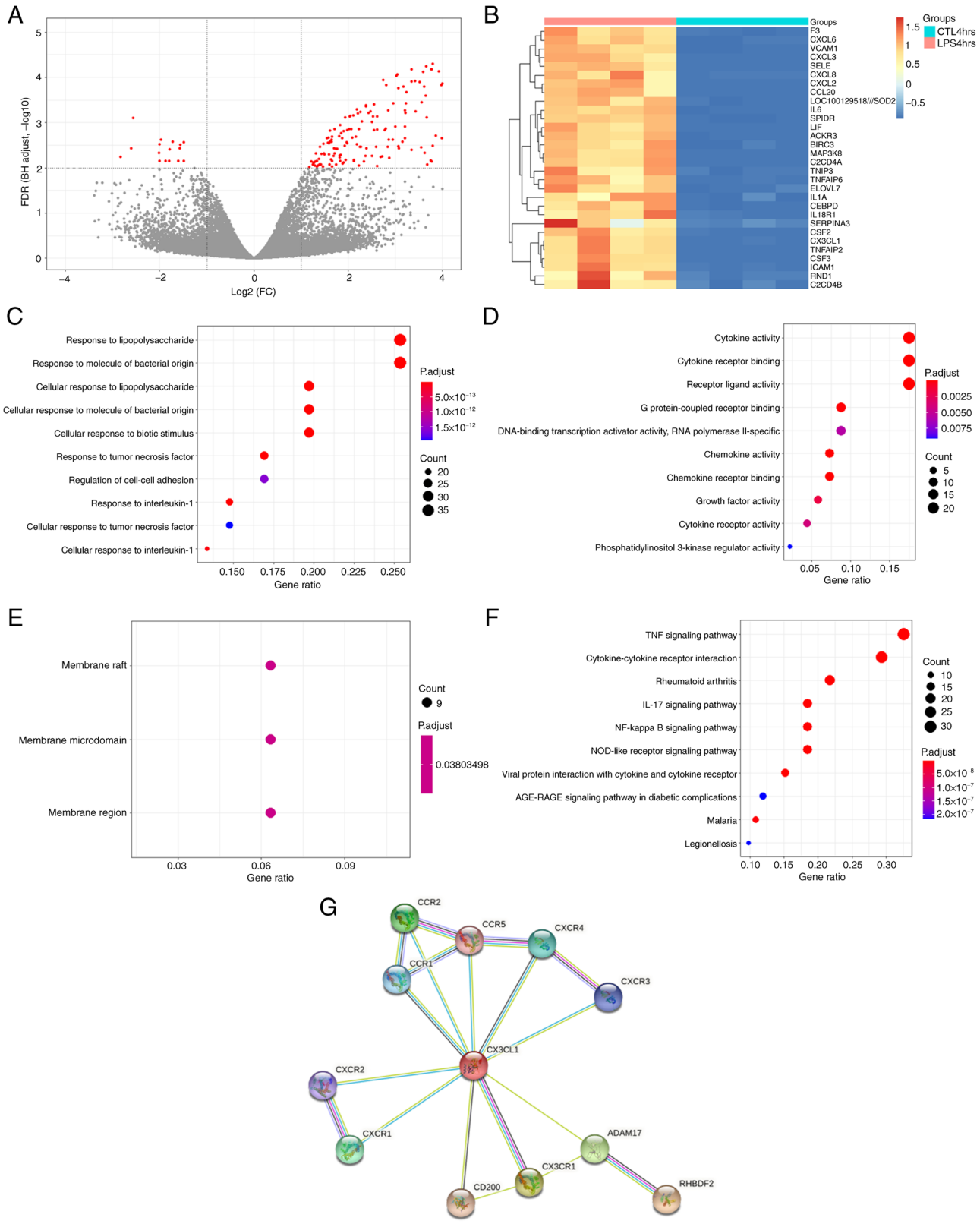

Figure 1. Bioinformatics analysis. (A) DEGs, including 187 upregulated and 16 downregulated genes. (B) Top 30 upregulated DEGs which included CX3CL1. (C) Biological process, (D) molecular function and (E) cell component Gene Ontology enrichment analysis. (F) Kyoto Encyclopedia of Genes and Genomes enrichment analysis. (G) Interaction between iRHOM2 and CX3CL1 genes using a protein-protein interaction network. DEG, differentially expressed gene; FDR, false discovery rate; FC, fold-change; iRHOM2, inactive rhomboid-like protein 2; CX3CL1, C-X3-C motif chemokine ligand 1; LPS, lipopolysaccharide; CTL, control.

the role of iRHOM2 in endothelial barrier permeability and expression levels of ZO-1, VE-cadherin and Occludin, endothelial permeability measurement and an IF assay for ZO-1 expression, as well as western blotting for the detection

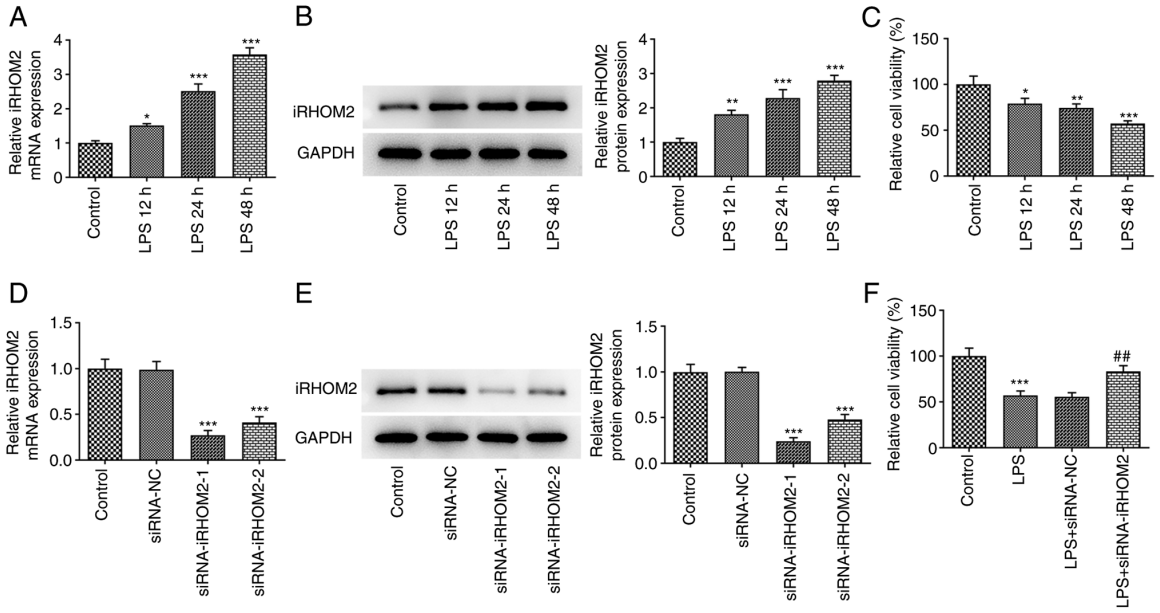

Figure 2. LPS induces increased expression of iRHOM2. (A) RT-qPCR analysis of iRHOM2 expression level in HPMVECs in response to LPS induction. (B) Western blot analysis of iRHOM2 expression levels in HPMVECs in response to LPS induction. (C) Cell Counting Kit-8 assay showed that LPS treatment decreased cell viability. (D) Transfection with siRNA-iRHOM2 decreased (E) iRHOM2 expression levels. (F) iRHOM2 silencing increased cell viability in LPS-stimulated HPMVECs. Data are presented as the mean ± standard deviation of three independent experiments performed in triplicate. *P<0.05, **P<0.01 and ***P<0.001 vs. control. $^{\#\#}$P<0.01 vs. LPS + siRNA-NC. iRHOM2, inactive rhomboid-like protein 2; siRNA, small interfering RNA; NC, negative control; LPS, lipopolysaccharide; HPMVEC, human pulmonary microvascular endothelial cell.

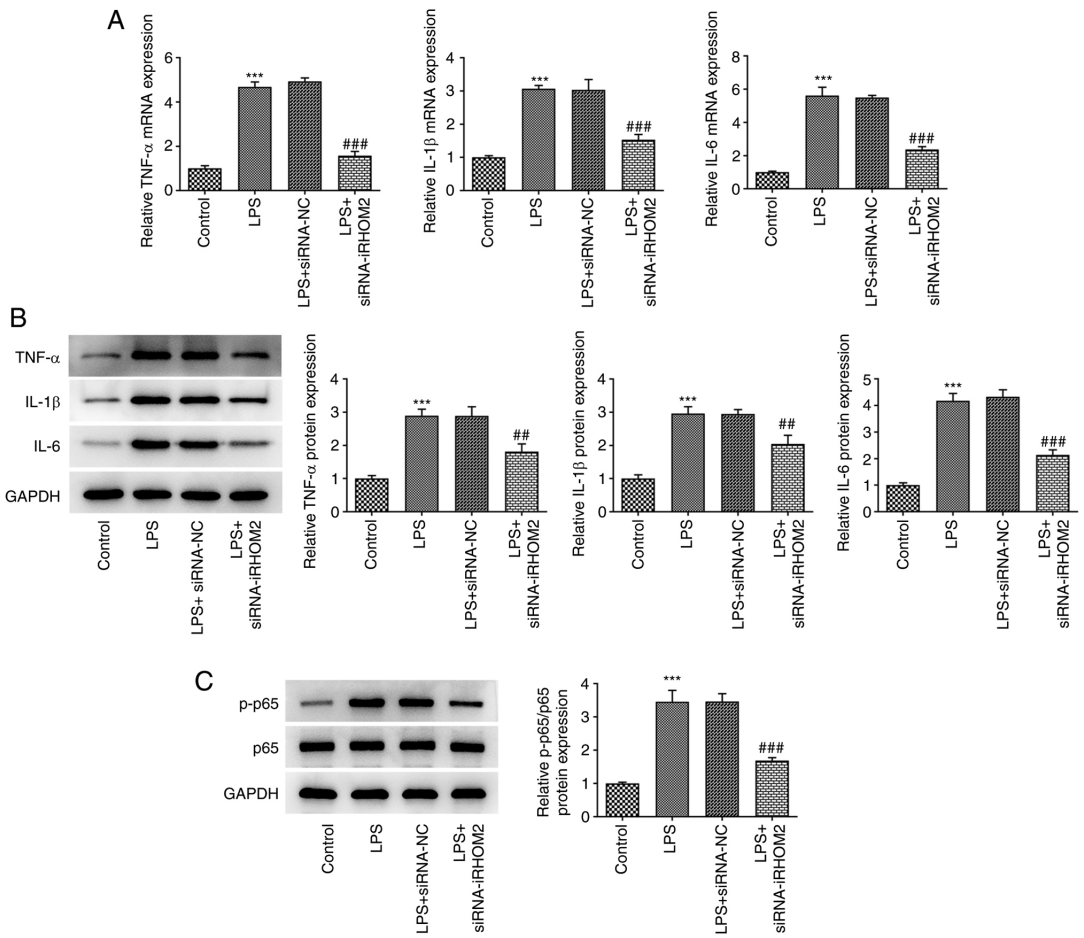

Figure 3. iRHOM2 silencing decreases inflammation and apoptosis. (A) Reverse transcription-quantitative PCR analysis of TNF-α, IL-1β and IL-6 mRNA expression. Western blot analysis of (B) TNF-α, IL-1β and IL-6 and (C) p-p65 and p65 expression. Data are presented as the mean ± standard deviation of three independent experiments performed in triplicate. ***P<0.001 vs. control. $^{\#\#}$P<0.01 and $^{\#\#\#}$P<0.001 vs. LPS + siRNA-NC. iRHOM2, inactive rhomboid-like protein 2; siRNA, small interfering RNA; NC, negative control; LPS, lipopolysaccharide; p, phosphorylated.

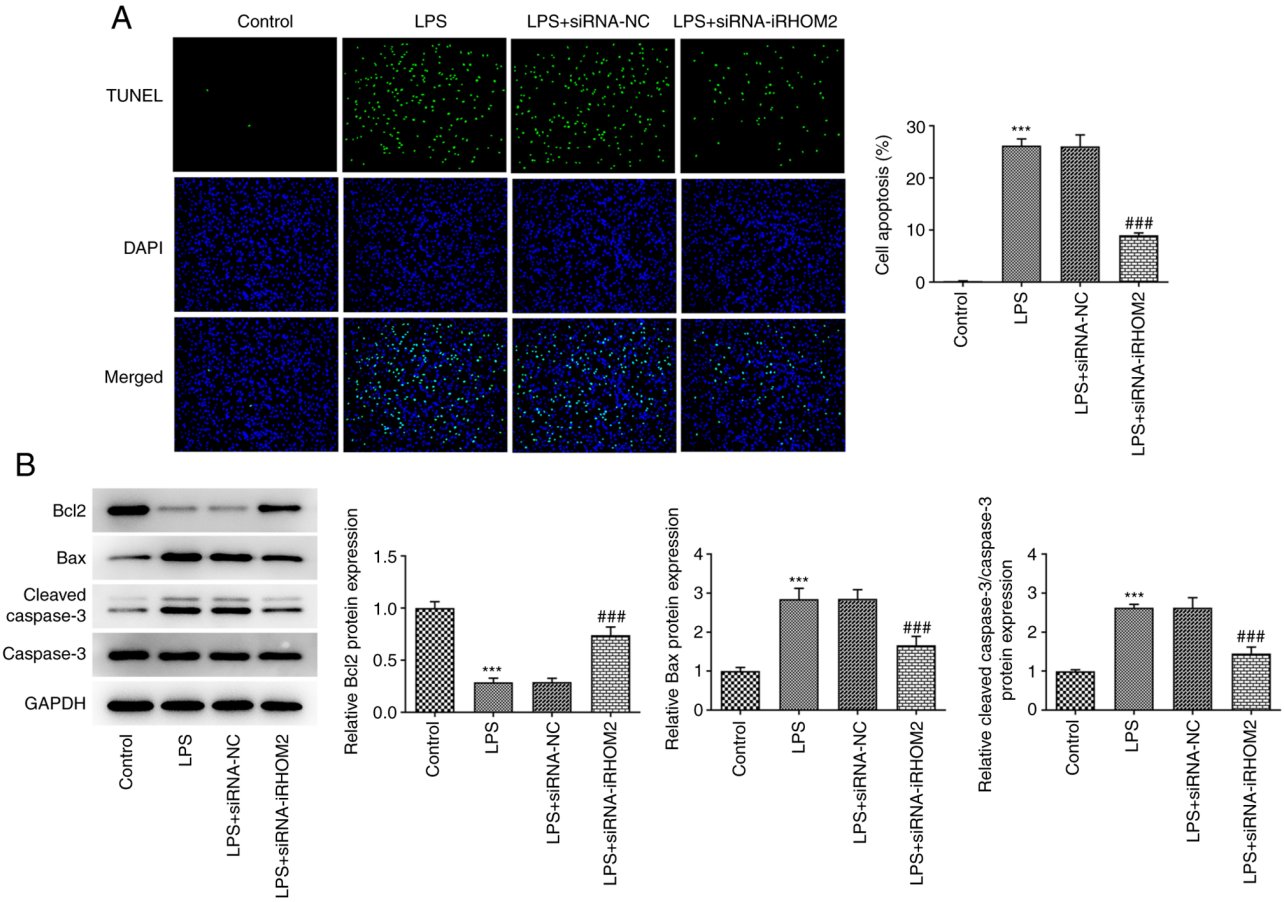

Figure 4. iRHOM2 silencing decreases apoptosis. (A) TUNEL assay analysis of apoptotic levels (magnification, x100). (B) Western blotting of Bcl-2, Bax and cleaved caspase 3 protein expression. Data are presented as the mean ± standard deviation of three independent experiments performed in triplicate. ***P<0.001 vs. control. ###P<0.001 vs. LPS + siRNA-NC. iRHOM2, inactive rhomboid-like protein 2; siRNA, small interfering RNA; NC, negative control; LPS, lipopolysaccharide.

of tight junction proteins, were performed. A decrease in TEER was observed following LPS induction compared with that in the control group and this effect was recovered by iRHOM2 silencing (Fig. 5A). Increased ZO-1 staining was observed, accompanied by the upregulation of expression levels of ZO-1, VE-cadherin and occludin in the LPS and siRNA-iRHOM2 co-treatment group compared with the LPS and siRNA-NC co-treatment group (Fig. 5B and C).

iRHOM2 interference inhibits CX3CL1 expression in LPS-induced HPMVECs. The present study investigated if the aforementioned effects of iRHOM2 were due to changes in CX3CL1 expression. CX3CL1 expression was measured using RT-qPCR and western blotting. Upregulation of CX3CL1 expression at both mRNA and protein levels was observed in HPMVECs in response to LPS treatment (Fig. 6A and B). Furthermore, iRHOM2 silencing promoted CX3CL1 expression compared with the siRNA-NC group of LPS-treated HPMVECs (Fig. 6C and D). Furthermore, there was an interaction between iRHOM2 and CX3CL1 (Fig. 6E and F).

iRHOM2 interference alters cell viability, inflammation, apoptosis and endothelial integrity via CX3CL1. To determine the regulatory role of iRHOM2 in cell viability, inflammation and apoptosis, CX3CL1 overexpression was induced by transfection of Ov-CX3CL1 into HPMVECs. Increased expression levels of CX3CL1 were observed following Ov-CX3CL1 transfection compared with those in the control (Fig. 7A and B). The present study examined whether CX3CL1 mediated the role of iRHOM2 in LPS-induced HPMVECs. It was found that the viability in LPS + siRNA-iRHOM2 group was reduced after overexpressing CX3CL1 (Fig. 7C). Compared with LPS + siRNA-iRHOM2 + Ov-NC group, CX3CL1 overexpression increased the expressions of TNF-α, IL-1β and IL-6 in LPS-induced HPMVECs transfected with siRNA-iRHOM2 (Figs. 7D-E). The decreased mRNA and protein expressions of p-p65 in LPS-induced due to iRHOM2 silence were increased by CX3CL1 overexpression (Fig. 7F). Compared with LPS + siRNA-iRHOM2 + Ov-NC group, CX3CL1 overexpression promoted the cell apoptosis, accompanied by decreased Bcl-2 expression and increased expressions of Bax and cleaved caspase3 (Figs. 8A-B). However, this effect was reversed in the LPS, siRNA-iRHOM2 and Ov-CX3CL1 co-treatment groups. Furthermore, CX3CL1 overexpression reversed the effect of iRHOM2 silencing on TEER levels and expression levels of ZO-1, VE-cadherin and occludin (Fig. 9A-C), suggesting that iRHOM2/CX3CL1 affected endothelial integrity.

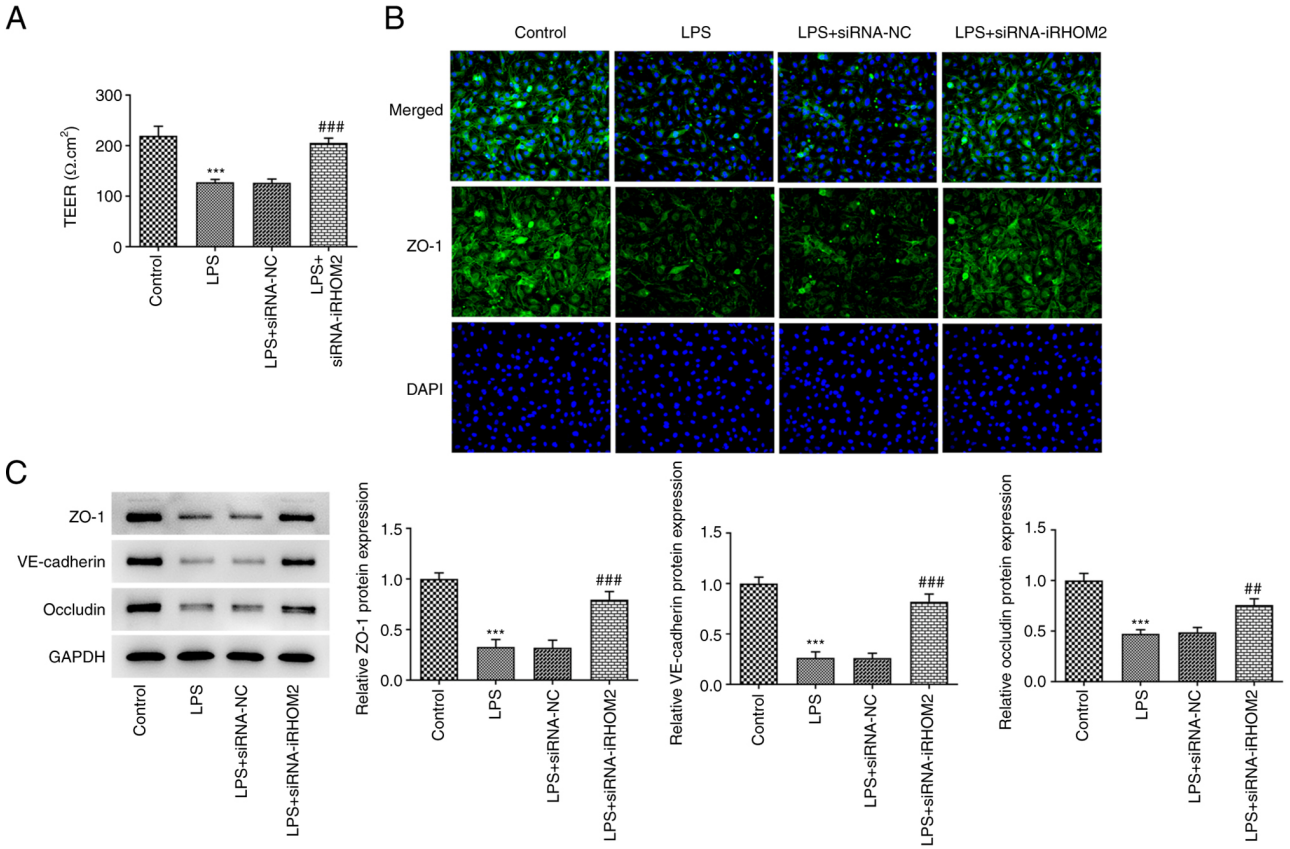

Figure 5. iRHOM2 silencing maintains endothelial integrity. (A) Analysis of endothelial barrier permeability using TEER measurement. (B) Immunofluorescence staining assay for ZO-1 protein expression (Magnification, x100). (C) Protein expression of ZO-1, VE-cadherin and occludin was increased by iRHOM2 silencing following LPS challenge. Data are presented as the mean ± standard deviation of three independent experiments performed in triplicate. ***P<0.001 vs. control. $^{##}$P<0.01, $^{###}$P<0.001 vs. LPS + siRNA-NC. ZO-1, zonula occludens-1; iRHOM2, inactive rhomboid-like protein 2; siRNA, small interfering RNA; NC, negative control; LPS, lipopolysaccharide; VE, vascular-endothelial; TEER, transendothelial electrical resistance.

Discussion

CX3CL1 is a unique chemokine that can exist in a soluble form, as a chemotactic cytokine, or in a membrane-attached form that serves as a binding molecule (18). A previous study demonstrated that Baicalin, a type of flavonoid, exerts protective effects against LPS-induced ALI by regulating the CX3CL1/CX3CR1 axis and NF-κB pathway in CX3CL1-knockout mice (19). The present bioinformatics analysis showed that CX3CL1 expression was upregulated in the LPS group compared with that in the control group. KEGG pathway analysis demonstrated that the TNF signaling pathway affected by iRHOM2 and cytokine-cytokine receptor interaction, including CX3CL1, was involved in ALI. To the best of our knowledge, however, the specific roles of CX3CL1 in ALI and the association between CX3CL1 and iRHOM2 have not reported yet. iRHOM2 is a key cofactor for TNF-α-converting enzyme, the metalloprotease that removes both the proinflammatory cytokine TNF-α and TNF receptors (TNFRs) from the cell surface (20). PPI network analysis revealed no direct association between iRHOM2 and CX3CL1. However, the present study showed that iRHOM2 could interact with CX3CL1 by IP assay. The present study demonstrated that, following LPS induction and iRHOM2 silencing, HPMVECs exhibited enhanced cell viability, decreased pro-inflammatory factor expression and apoptosis levels and improved endothelial barrier permeability compared with HPMVECs only treated with LPS. However, CX3CL1 overexpression counteracted the effects of iRHOM2 silencing on LPS-induced HPMVECs. Given the interaction of iRHOM2 and CX3CL1, LPS treatment led to inflammation, apoptosis and the alteration of endothelial barrier permeability that were potentially associated with iRHOM2 upregulation and CX3CL1 downregulation. The present study used the total form of VE-cadherin to evaluate VE cell permeability (21-23). p-VE-cadherin may also be a marker of VE cell permeability and should be detected in future studies (24,25).

The present study demonstrated that iRHOM2 silencing led to decreased levels of TNFα, IL-1β and IL-6 in HPMVECs stimulated with LPS, accompanied by decreased phosphorylation of p65. Previous studies have shown that iRHOM2 participates in the regulation of inflammation (7,26,27). A recent report demonstrated that inhibition of iRHOM2/NF-κB signaling is involved in suppressing inflammation (28). The present study identified an interaction between iRHOM2 and CX3CL1 and found that CX3CL1 overexpression inhibited the protective effects of iRHOM2 silencing against LPS-induced cell injury. In response to LPS stimulation, endothelial cells overproduce pro-inflammatory chemokines, including CX3CL1 (29). Adult patients with sepsis exhibit increased CX3CL1 expression, which is positively associated with inflammatory cytokines, such as IL-6, IL-1β and TNF-α (30).

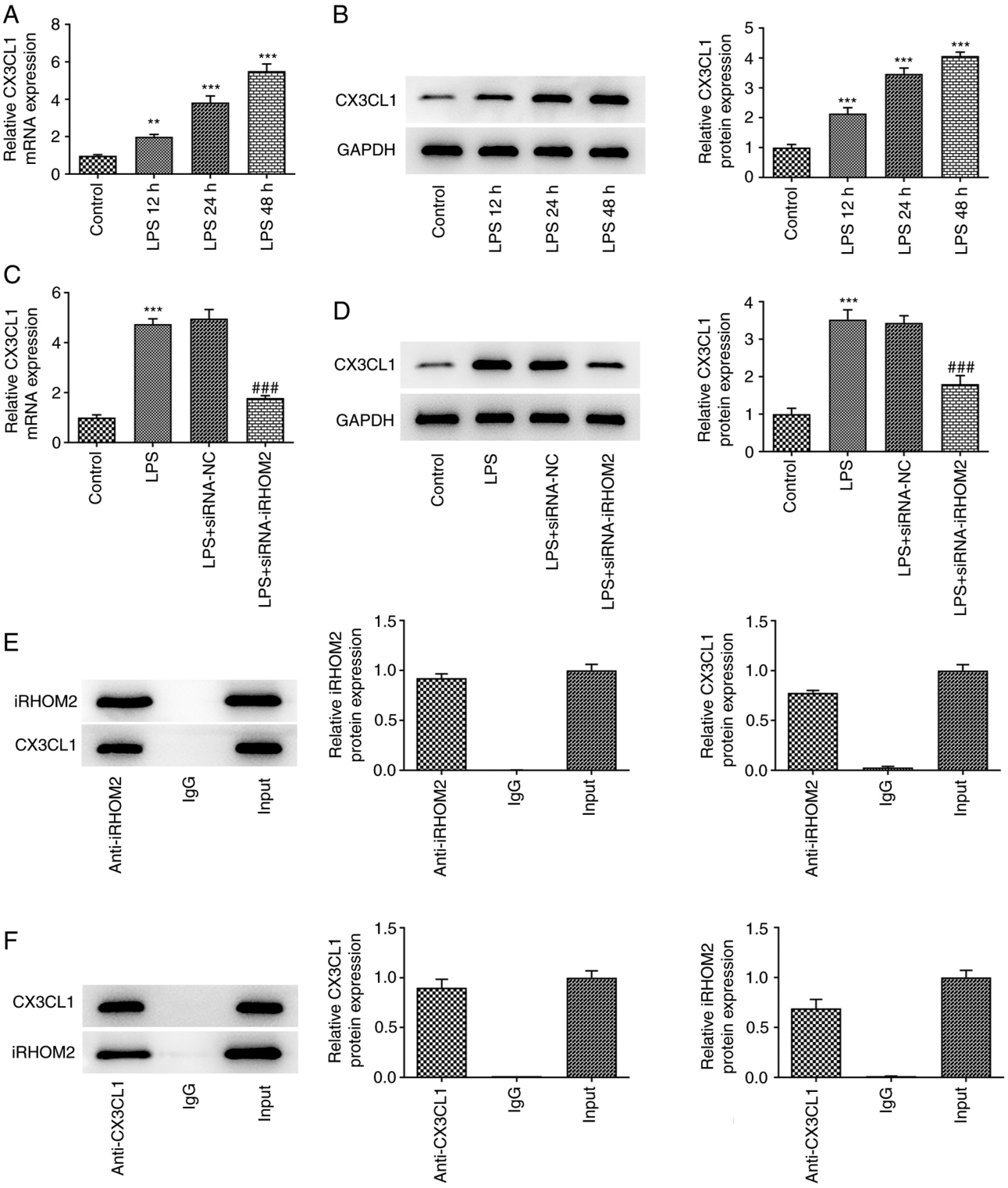

Figure 6. CX3CL1 expression is decreased by iRHOM2 interference in LPS-treated human pulmonary microvascular endothelial cells. (A) RT-qPCR analysis of CX3CL1 expression in response to LPS stimulation. (B) Western blot analysis of CX3CL1 in response to LPS stimulation. (C) Reverse transcription-quantitative PCR analysis was performed to measure mRNA expression of CX3CL1. (D) Western blot assay was performed to measure protein levels of CX3CL1. (E) Immunoprecipitation assay showed the existence of CX3CL1 in anti-iRHOM2. (F) Immunoprecipitation assay showed the existence of iRHOM2 in anti-CX3CL1. association between iRHOM2 and CX3CL1. Data are presented as the mean ± standard deviation of three independent experiments performed in triplicate. **P<0.01, ***P<0.001 vs. control. $^{###}$P<0.001 vs. LPS + siRNA-NC. RT-qPCR, reverse transcription-quantitative polymerase chain reaction; CX3CL1, C-X3-C motif chemokine ligand 1; iRHOM2, inactive rhomboid-like protein 2; siRNA, small interfering RNA; NC, negative control; LPS, lipopolysaccharide.

CX3CL1 blockade leads to alleviation of lung injury in cecal ligation and puncture-induced sepsis (30). However, the present study did not use CX3CL receptor inhibitors; use of CX3CL receptor inhibitors to block the effects of CX3CL should be explored in future studies. Moreover, the effects of CX3CL on iRHOM2-regulated ALI should also be investigated in further

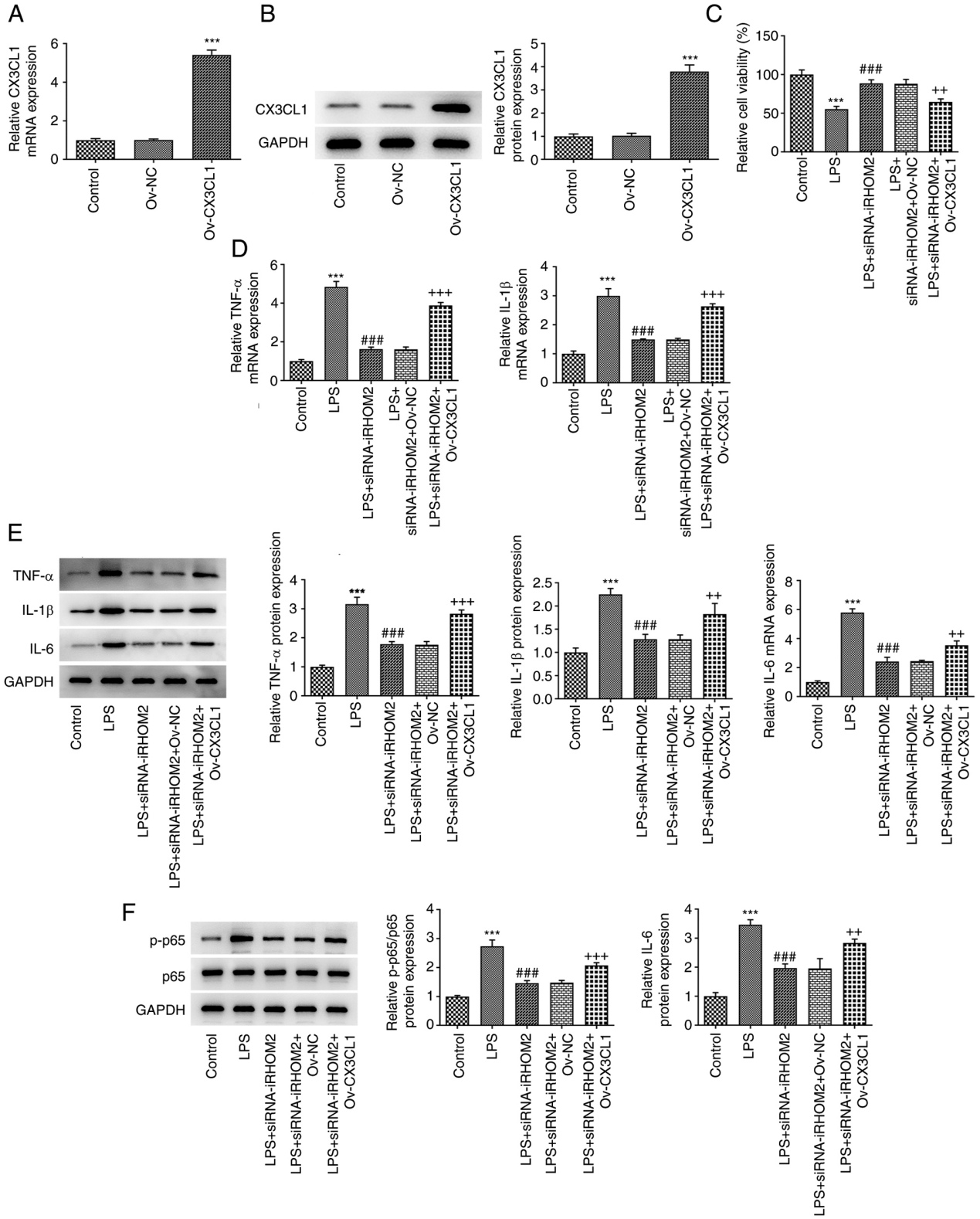

Figure 7. iRHOM2 interacts with CX3CL1 to affect cell viability and inflammation and apoptosis in response to LPS. (A) Reverse transcription-quantitative PCR analysis was performed to measure mRNA expression of CX3CL1. (B) Western blot assay was performed to measure protein levels of CX3CL1. ***P<0.001 vs. Ov-NC. (C) Cell Counting Kit-8 assay showed cell viability. (D) RT-qPCR analysis of TNF-α, IL-1β and IL-6 expressions. (E) Western blot analysis of TNF-α, IL-1β and IL-6 expressions. (F) Western blot analysis of the p-p65 and p65 protein levels. Data are presented as the mean ± standard deviation of three independent experiments performed in triplicate. ***P<0.001 vs. control. $^{###}$P<0.001 vs. LPS. $^{+}$P<0.05, $^{++}$P<0.01 and $^{+++}$P<0.01 vs. LPS + siRNA-iRHOM2 + Ov-NC. RT-qPCR, reverse transcription-quantitative polymerase chain reaction; CX3CL1, C-X3-C motif chemokine ligand 1; iRHOM2, inactive rhomboid-like protein 2; siRNA, small interfering RNA; NC, negative control; LPS, lipopolysaccharide; Ov-, overexpression; p, phosphorylated.

study. In addition, to the best of our knowledge, the majority of LPS-associated experiments use 12-48 h for LPS treatment to treat cells (31-33). Thus, the present study used 12, 24 and 48 h as LPS treatment duration. Moreover, the present study found

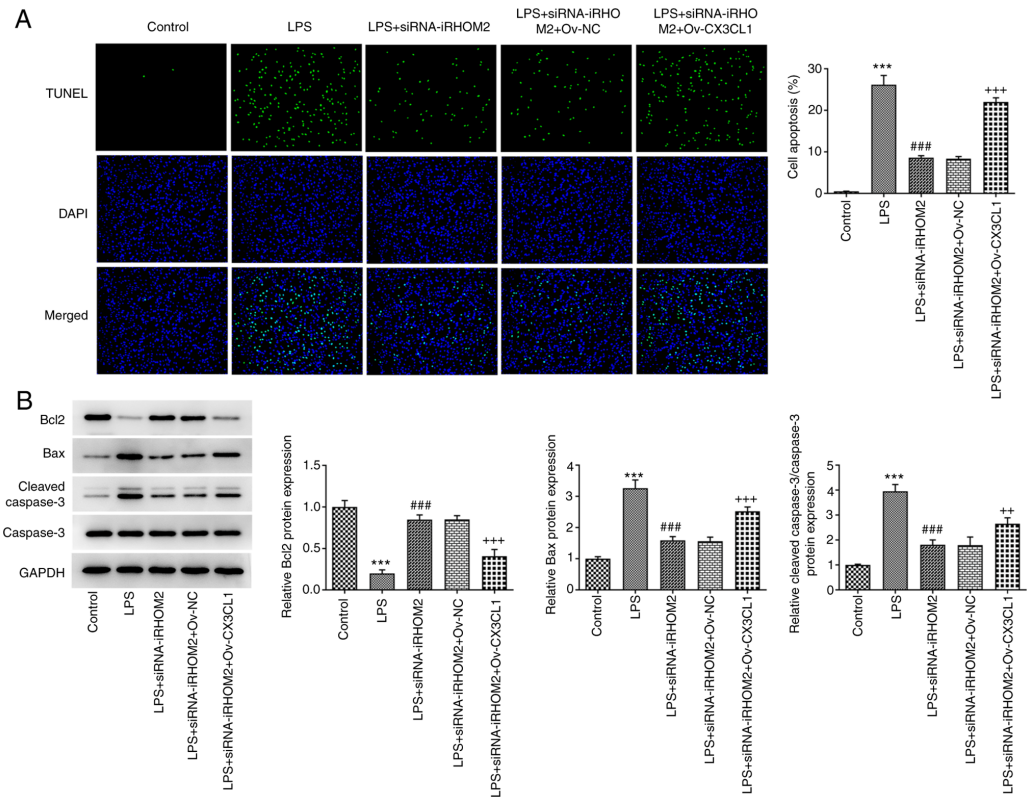

Figure 8. iRHOM2 interacts with CX3CL1 to affect apoptosis in response to LPS treatment. (A) Apoptosis levels were measured using TUNEL assay. (Magnification, x100). (B) Western blotting was performed for measurement of Bcl-2, Bax and cleaved caspase3 protein levels. Data are presented as the mean ± standard deviation of three independent experiments performed in triplicate. ***P<0.001 vs. control. $^{###}$P<0.001 vs. LPS. $^{++}$P<0.01 and $^{+++}$P<0.01 vs. LPS + siRNA-iRHOM2 + Ov-NC. CX3CL1, C-X3-C motif chemokine ligand 1; iRHOM2, inactive rhomboid-like protein 2; siRNA, small interfering RNA; NC, negative control; LPS, lipopolysaccharide; Ov, overexpression.

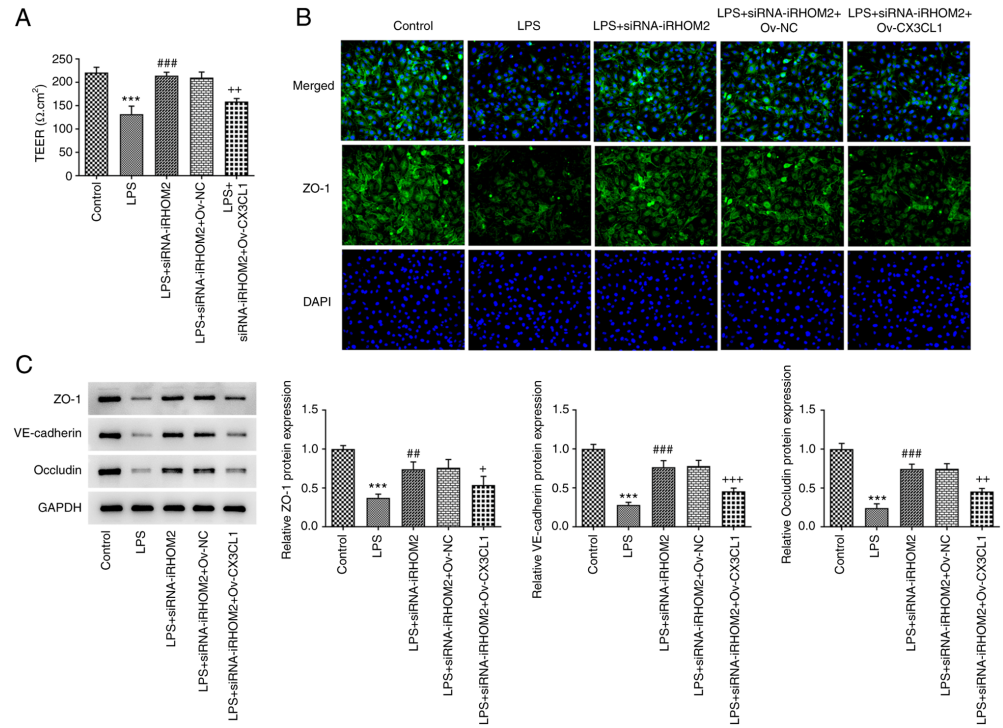

Figure 9. iRHOM2 interacts with CX3CL1 to affect endothelial integrity in LPS-induced human pulmonary microvascular endothelial cells. (A) Analysis of endothelial barrier permeability using TEER measurement. (B) Immunofluorescence staining for ZO-1 protein expression. (magnification, x100). (C) Western blot assay was performed to analyze protein expression of ZO-1, VE-cadherin and occludin. Data are presented as the mean ± standard deviation of three independent experiments performed in triplicate. ***P<0.001 vs. control. $^{##}$P<0.01 and $^{###}$P<0.001 vs. LPS. $^{+}$P<0.05, $^{++}$P<0.01 and $^{+++}$P<0.01 vs. LPS + siRNA-iRHOM2 + Ov-NC. ZO-1, zonula occludens-1; iRHOM2, inactive rhomboid-like protein 2; siRNA, small interfering RNA; NC, negative control; LPS, lipopolysaccharide; VE, vascular-endothelial; TEER, transendothelial electrical resistance.

that iRHOM2 regulated CX3CL1 expression and iRHOM2 silencing affected inflammation and endothelial barrier permeability via CX3CL1 but did not test the expression of iRHOM2 in CX3CL1-overexpressing cells. Therefore, further studies on the association between iRHOM2 and CX3CL1 and the role of iRHOM2 in CX3CL1-regulated cells should be performed in future.

In conclusion, the present data indicated that targeting iRHOM2/CXCL1 therapeutically may ameliorate the inflammation and improve endothelial barrier permeability. Further study of the mechanism of iRHOM2/CXCL1 will determine the regulatory role of these molecules in inflammation and endothelial barrier permeability.

Acknowledgements

Not applicable.

Funding

No funding was received.

Availability of data and materials

All data generated or analyzed during this study are included in this published article.

Authors' contributions

HLY and HYY designed the study and drafted and revised the manuscript. HLY, JSW and HYY analyzed the data, searched the literature and performed experiments. HLY and HYY confirm the authenticity of all the raw data All authors have read and approved the final manuscript.

Ethics approval and consent to participate

Not applicable.

Patient consent for publication

Not applicable.

Competing interests

The authors declare that they have no competing interests.

Reference

1. Schmidt GA: Managing Acute Lung Injury. Clin Chest Med 37: 647-658, 2016.
2. Lu Z, Li Y, Ru JH, Lopes-Virella MF, Lyons TJ and Huang Y: Interaction of palmitate and LPS regulates cytokine expression and apoptosis through sphingolipids in human retinal microvascular endothelial cells. Exp Eye Res 178: 61-71, 2019.
3. Yang J, Ruan F and Zheng Z: Ripasudil attenuates lipopolysaccharide (LPS)-mediated apoptosis and inflammation in pulmonary microvascular endothelial cells via ROCK2/eNOS Signaling. Med Sci Monit 24: 3212-3219, 2018.
4. Zyrianova T, Lopez B, Liao A, Gu C, Wong L, Ottolia M, Olcese R and Schwingshackl A: BK channels regulate LPS-induced CCL-2 release from human pulmonary endothelial cells. Am J Respir Cell Mol Biol 64: 224-234, 2021.
5. Wang X, Yan J, Xu X, Duan C, Xie Z, Su Z, Ma H, Ma H, Wei X and Du X: Puerarin prevents LPS-induced acute lung injury via inhibiting inflammatory response. Microb Pathog 118: 170-176, 2018.
6. Freeman M: Rhomboid proteases and their biological functions. Annu Rev Genet 42: 191-210, 2008.
7. Chaohui C, Wei H, Hongfeng W, Yueliang Z, Xiaoqin P, Pingli Z and Zhibing A: iRhom2 promotes atherosclerosis through macrophage inflammation and induction of oxidative stress. Biochem Biophys Res Commun 503: 1897-1904, 2018.
8. Badenes M, Amin A, González-García I, Félix I, Burbridge E, Cavadas M, Ortega FJ, de Carvalho É, Faísca P, Carobbio S, *et al*: Deletion of iRhom2 protects against diet-induced obesity by increasing thermogenesis. Mol Metab 31: 67-84, 2020.
9. Xu MX, Qin YT, Ge CX, Gu TT, Lou DS, Li Q, Hu LF, Li YY, Yang WW and Tan J: Activated iRhom2 drives prolonged $PM_{2.5}$ exposure-triggered renal injury in Nrf2-defective mice. Nanotoxicology 12: 1045-1067, 2018.
10. Lu XL, Zhao CH, Zhang H and Yao XL: iRhom2 is involved in lipopolysaccharide-induced cardiac injury in vivo and in vitro through regulating inflammation response. Biomed Pharmacother 86: 645-653, 2017.
11. Kim JH, Kim J, Chun J, Lee C, Im JP and Kim JS: Role of iRhom2 in intestinal ischemia-reperfusion-mediated acute lung injury. Sci Rep 8: 3797, 2018.
12. Ritchie ME, Phipson B, Wu D, Hu Y, Law CW, Shi W and Smyth GK: Limma powers differential expression analyses for RNA-sequencing and microarray studies. Nucleic Acids Res 43: e47, 2015.
13. Zhang C, Zheng Y, Li X, Hu X, Qi F and Luo J: Genome-wide mutation profiling and related risk signature for prognosis of papillary renal cell carcinoma. Ann Transl Med 7: 427, 2019.
14. von Mering C, Huynen M, Jaeggi D, Schmidt S, Bork P and Snel B: STRING: A database of predicted functional associations between proteins. Nucleic Acids Res 31: 258-261, 2003.
15. Livak KJ and Schmittgen TD: Analysis of relative gene expression data using real-time quantitative PCR and the 2(-Delta Delta C(T)) Method. Methods 25: 402-408, 2001.
16. Srinivasan B, Kolli AR, Esch MB, Abaci HE, Shuler ML and Hickman JJ: TEER measurement techniques for in vitro barrier model systems. J Lab Autom 20: 107-126, 2015.
17. Li S, Gao P, Dai X, Ye L, Wang Z and Cheng H: New prognostic biomarker CMTM3 in low grade glioma and its immune infiltration. Ann Transl Med 10: 206, 2022.
18. Liu W, Jiang L, Bian C, Liang Y, Xing R, Yishakea M and Dong J: Role of CX3CL1 in Diseases. Arch Immunol Ther Exp (Warsz) 64: 371-383, 2016.
19. Ding XM, Pan L, Wang Y and Xu QZ: Baicalin exerts protective effects against lipopolysaccharide-induced acute lung injury by regulating the crosstalk between the CX3CL1-CX3CR1 axis and NF-κB pathway in CX3CL1-knockout mice. Int J Mol Med 37: 703-715, 2016.
20. Badenes M and Adrain C: iRhom2 and TNF: Partners or enemies? Sci Signal 12: eaaz0444, 2019.
21. Yokota Y, Noda T, Okumura Y, Kobayashi S, Iwagami Y, Yamada D, Tomimaru Y, Akita H, Gotoh K, Takeda Y, *et al*: Serum exosomal miR-638 is a prognostic marker of HCC via downregulation of VE-cadherin and ZO-1 of endothelial cells. Cancer Sci 112: 1275-1288, 2021.
22. Jiang W, Sun Y, Wang H, Hu Z, Song J, Meng C, Duan S, Jiang Z, Yu Y and Hu D: HIF-1α Enhances Vascular Endothelial Cell Permeability Through Degradation and Translocation of Vascular Endothelial Cadherin and Claudin-5 in Rats With Burn Injury. J Burn Care Res 42: 258-268, 2021.
23. Gomez Perdiguero E, Liabotis-Fontugne A, Durand M, Faye C, Ricard-Blum S, Simonutti M, Augustin S, Robb BM, Paques M, Valenzuela DM, *et al*: ANGPTL4-αvβ3 interaction counteracts hypoxia-induced vascular permeability by modulating Src signalling downstream of vascular endothelial growth factor receptor 2. J Pathol 240: 461-471, 2016.
24. Smith RO, Ninchoji T, Gordon E, André H, Dejana E, Vestweber D, Kvanta A and Claesson-Welsh L: Vascular permeability in retinopathy is regulated by VEGFR2 Y949 signaling to VE-cadherin. Elife 9: e54056, 2020.
25. Liu J, Miao G, Wang B, Zheng N, Ma L, Chen X, Wang G, Zhao X, Zhang L and Zhang L: Chlamydia pneumoniae infection promotes monocyte transendothelial migration by increasing vascular endothelial cell permeability via the tyrosine phosphorylation of VE-cadherin. Biochem Biophys Res Commun 497: 742-748, 2018.

26. Zhou C, Chen R, Gao F, Zhang J and Lu F: 4-Hydroxyisoleucine relieves inflammation through iRhom2-dependent pathway in co-cultured macrophages and adipocytes with LPS stimulation. BMC Complement Med Ther 20: 373, 2020.
27. Zhou C, Qin Y, Chen R, Gao F, Zhang J and Lu F: Fenugreek attenuates obesity-induced inflammation and improves insulin resistance through downregulation of iRhom2/TACE. Life Sci 258: 118222, 2020.
28. Chenxu G, Xianling D, Qin K, Linfeng H, Yan S, Mingxin X, Jun T and Minxuan X: Fisetin protects against high fat diet-induced nephropathy by inhibiting inflammation and oxidative stress via the blockage of iRhom2/NF-κB signaling. Int Immunopharmacol 92: 107353, 2021.
29. Jiang R, Wei L, Zhu M, Wu J and Wang L: Aspirin Inhibits LPS-Induced Expression of PI3K/Akt, ERK, NF-κB, CX3CL1, and MMPs in human bronchial epithelial cells. Inflammation 39: 643-650, 2016.
30. Chen X, Wei Q, Hu Y and Wang C: Role of Fractalkine in promoting inflammation in sepsis-induced multiple organ dysfunction. Infect Genet Evol 85: 104569, 2020.
31. Zhang Y, Yan M, Yu QF, Yang PF, Zhang HD, Sun YH, Zhang ZF and Gao YF: Puerarin Prevents LPS-Induced osteoclast formation and bone loss via inhibition of Akt activation. Biol Pharm Bull 39: 2028-2035, 2016.
32. Abarca-Vargas R and Petricevich VL: Extract from Bougainvillea xbuttiana (Variety Orange) Inhibits Production of LPS-Induced inflammatory mediators in macrophages and exerts a protective effect in vivo. Biomed Res Int 2019: 2034247, 2019.
33. Suzuki K, Okada H, Takemura G, Takada C, Kuroda A, Yano H, Zaikokuji R, Morishita K, Tomita H, Oda K, *et al*: Neutrophil elastase damages the pulmonary endothelial glycocalyx in lipopolysaccharide-induced experimental endotoxemia. Am J Pathol 189: 1526-1535, 2019.